Linear optical properties of zigzag single-walled BN nanotube ensembles from a model calculation

Vl. A. Margulis*
Department of Physics, N. P. Ogarev Mordovian State University, Saransk 430000, Russia

E. A. Gaiduk, E. E. Muryumin, O. V. Boyarkina, and L. V. Fomina
Department of Chemistry, N. P. Ogarev Mordovian State University, Saransk 430000, Russia
(Received 6 October 2006; published 15 December 2006)

We present a simple theoretical description of the linear optical properties of zigzag single-walled BN nanotube (BN-SWNT) ensembles within a single-particle approach that uses the Král-Mele-Tománek effective Hamiltonian for modeling the electronic structure of such tubes. The perturbation-theory method of Genkin and Mednis is applied to derive analytical expressions for both the real and imaginary parts of the linear optical susceptibility $\chi^{(1)}(\omega)$, and these are used to calculate numerically the optical functions (dielectric function, refractive index, reflectance and optical absorption coefficient) for several representative BN-SWNT ensembles. The results of our calculations are discussed in the light of the recent experimental observation by Lauret *et al.* [Phys. Rev. Lett. **94**, 037405 (2005)] of the optical absorption spectrum of an assemble of large-diameter BN-SWNT's. It is shown that the developed theory is capable of explaining the dominant features of the experimental data, thus suggesting that the characteristic peaks observed in the optical absorption spectrum of BN-SWNT's are due to direct interband electron transitions between pairs of van Hove singularities in the electronic density of states of these tubes.

DOI: 10.1103/PhysRevB.74.245419 PACS number(s): 78.67.Ch, 78.30.Fs, 78.40.Fy

I. INTRODUCTION

Although boron nitride nanotubes (BNNT's) were first predicted theoretically and successfully synthesized more than a decade ago,[1–4] their optical properties are only starting to be explored. Recently, Lauret *et al.*[5] have measured the optical absorption spectrum for an assembly of single-walled BN nanotubes (BN-SWNT's) with an average diameter of about 1.4 nm. The observed spectrum consists of three broad absorption bands with the peak energies at 4.45, 5.5, and 6.15 eV and with the increasing peak intensity on going over to the high-energy side. It has also been observed that the lowest absorption band can be decomposed into two substructures centered at 4.4 and 4.5 eV, respectively.

In Ref. 5, two possible interpretations of the above-mentioned spectral features have been discussed. The first interpretation is based on a simple noninteracting electron model in which the optical resonances arise from interband electron transitions. The second interpretation, on the contrary, suggests that a one-dimensional exciton effect plays an important role in determining the optical transition energies. While a definitive test for both of the above-mentioned models has not been provided in Ref. 5, the authors of that paper have assumed that at least the lowest absorption band in the observed spectrum should be attributed to the formation of excitons rather than free electron-hole pairs.

A number of theoretical studies have also been reported on the optical properties of BNNT's, mainly of fairly small diameters.[6–10] Ng and Zhang[6] used a semiempirical localized-density matrix approach to calculate the optical properties of a few BN-SWNT's. However, their optical absorption spectra, as given in Ref. 6, show only one major peak below 6 eV, which is quite different from the two-peak structure of the spectrum observed in experiment.[5] Marinopoulos *et al.*[7] as well as Guo and Lin[8] carried out density-functional-theory calculations of the optical properties of BN-SWNT's on the basis of both the local density and random phase approximations—i.e., without considering many-electron effects. The optical absorption spectra presented in Refs. 7 and 8 are also markedly different from the experimental spectrum measured by Lauret *et al.*[5] Two more recent papers of Park *et al.*[9] and Wirtz *et al.*[10] have reported first-principles calculations of the effect of electron-electron and electron-hole interections on the optical absorption spectra of BN-SWNT's. According to their calculations the optical response of BN-SWNT's is strongly dominated by excitonic effects. However, both these studies have been focused on a few selected small-diameter BN-SWNT's, and no results have been obtained for BN-SWNT's with diameter similar to the average diameter $d_{av}=1.4$ nm of the tubes used in the experiment,[5] probably owing to the limitation of computer resources. This makes very difficult a direct comparison between theory and experiment. Nevertheless, in Ref. 10 it was claimed that both alternatives (the interband and the excitonic transitions) discussed in Ref. 5 fail to explain the nature of the two peaks at 4.45 and 5.5 eV in the absorption spectrum. How then can we understand the experimental results?

Further experimental and theoretical work is evidently highly desirable in order to overcome this difficulty. On the theoretical side, what is first of all needed is a unified treatment of the optical properties of BN-SWNT's of different diameters, including 1.4 nm-mean-diameter tubes used in the experiment.[5] It is, of course, desirable that such a treatment would not require significant computational labor to carry out numerical calculations of optical functions. The *ab initio* many-electron Green's function approach elaborated on in Refs. 9 and 10, though remarkably accurate, can scarcely be

applied to the study of a wide range of large-diameter tubes, since it requires extensive computational power, which is not available at present. This provides the motivation for the present study in which we analyze the linear optical properties of BN-SWNT's based on a simplified, but analytically tractable, one-electron model proposed by Král and co-workers[11,12] to describe the band structure of BN-SWNT's within an effective-mass approximation. The advantage of the approach is that it enables an explicit expression to be obtained for the complex dielectric function of BN-SWNT's. The numerical calculations of the optical functions, such as refractive index, optical absorption coefficient, and reflectance, are then readily implemented for BN-SWNT's of different diameters. A detailed analysis of the spectral behavior of these functions, which has not yet been reported the literature, is the focus of the present study.[13] We are particularly interested in investigating to what extent the simple model approach, in which excitonic effects are disregarded, can explain the experiment on the optical absorption of BN-SWNT's.[5] The results of our calculations show that rather close agreement with experiment can be achieved already within a single-electron approach. This indicates that one-photon absorption spectroscopy is probably far from being an ideal tool to discriminate between the two above-mentioned alternative pictures (the free electron-hole pairs and the excitons) proposed for the interpretation of the experimental data—the situation closely resembling that observed for single-walled carbon nanotubes (see Refs. 14–20).

The rest of the paper is arranged as follows. In Sec. II we describe the theoretical scheme used to evaluate the optical functions of BN-SWNT's. A series of numerical studies of these functions is given in Sec. III. Our results for the optical absorption spectra are also presented in this section and compared with the experimental data obtained in Ref. 5. Finally, our conclusions are collected in Sec. IV.

II. THEORETICAL DESCRIPTION

We first specify the model adopted in the present paper. The system we are considering represents an ensemble of very closely packed and well-aligned, identical BN-SWNT's. Their geometrical structure (see Fig. 1) is specified by a chiral vector

$$\mathbf{C} = l_1\mathbf{a}_1 + l_2\mathbf{a}_2, \tag{1}$$

where $\mathbf{a}_1 = a_0(1,0)$ and $\mathbf{a}_2 = a_0(-1/2, \sqrt{3}/2)$ are the primitive lattice translation vectors of a two-dimensional BN sheet rolled up into a cylindrical form ($a_0 = 2.504$ Å is the lattice constant of the hexagonal BN). A set of two integers (l_1, l_2) uniquely determines the type of the nanotubes under consideration—i.e., their symmetry and radius. The latter is defined as

$$R = \frac{a_0}{2\pi}\sqrt{l_1^2 + l_2^2 - l_1 l_2}. \tag{2}$$

It was reported that BNNT's prefer a zigzag structure during their growth in current synthesis processes.[21,22] Therefore, our further treatment will be restricted to the zigzag

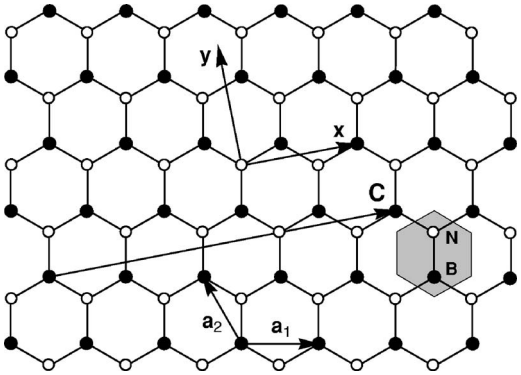

FIG. 1. Fragment of a two-dimensional BN sheet with B and N occupying alternate sites, which is rolled up in order to construct a BN-SWNT specified by a chiral vector **C**. Also shown the Cartesian coordinate axes x and y with the x direction along the circumference of the tube and the y direction along the axis of the tube. The vectors $\mathbf{a}_1$ and $\mathbf{a}_2$ with length a_0 are primitive translation vectors. The shaded hexagon represents a unit cell of the BN sheet.

BN-SWNT's with chiral index $(l,0)$. To describe their electronic structure we use the Král-Mele-Tománek (KMT) model[11] based on an effective-mass approximation and developed in the context of a simple tight-binding theory for π electrons. The KMT model treats only the electronic states near the conduction (c) and valence (v) band edges at K and K' points of the two-dimensional Brillouin zone of the BN sheet. The effective $\mathbf{k}\cdot\mathbf{p}$ Hamiltonian for these states associated with the K point can be represented in the form [cf. Eq. (1) in Ref. 11]

$$H = \sigma_z\Delta - i\gamma(\sigma_x\partial_x + \sigma_y\partial_y), \tag{3}$$

where σ_x, σ_y, and σ_z are the Pauli spin matrices, $\partial_x(\partial_y)$ stands for a partial derivative with respect to $x(y)$, $\gamma = \sqrt{3}|V_{pp\pi}|a_0/2$ is the $\mathbf{k}\cdot\mathbf{p}$ interaction parameter ($V_{pp\pi}$ is the π-electron transfer integral), and Δ is a site diagonal potential that distinguishes the B and N sites. Thus, γ and Δ are the two essential parameters that describe the KMT model.

In view of the simplicity of the model, the energy eigenvalues and the corresponding eigenstates of H in Eq. (3) are available in analytical form. Choosing axes x and y along the circumference of a nanotube and its symmetry axis, respectively, and imposing a periodic boundary condition in the x direction, we obtain the π electron energy dispersion in the vicinity of the K point as follows:

$$\varepsilon_{s\mathbf{k}} = \varepsilon_{s\nu mk} = \pm\sqrt{\Delta_{\nu m}^2 + \gamma^2 k^2}, \tag{4}$$

with

$$\Delta_{\nu m}^2 = \Delta^2 + \gamma^2\kappa_{\nu m}^2, \tag{5}$$

where $s(=c,v)$ is the band index, $\nu(=0,\pm1)$ is the number specified by the relation $l=3M+\nu$ with integer M, the azimuthal quantum number $m=0,\pm1,\pm2,\ldots,\pm(l-1)$ labels the size-quantized energy subbands, and $\mathbf{k}$ is the electron wave vector with two components: k_x and k_y. The former is quantized to the allowed discrete values

$$\kappa_{\nu m} = \frac{1}{3R}(3m - \nu), \tag{6}$$

while the latter (further labeled simply k) remains continuous for an infinitely long nanotube and takes values within the one-dimensional Brillouin zone $-k_{\mathrm{BZ}} \leqslant k \leqslant k_{\mathrm{BZ}}$, where $k_{\mathrm{BZ}} = \pi/a_0\sqrt{3}$. The upper (lower) sign on the right-hand side of Eq. (4) corresponds to the $c(v)$ band. The energy bands associated with the K' point are obtained by the replacement $\nu \to -\nu$ in Eq. (4).

The eigenstates of the Hamiltonian H in Eq. (3), corresponding to the two above-mentioned bands, are given by the following pseudospinors:[11]

$$\Phi_{c\mathbf{k}} = \begin{pmatrix} \Phi_{c\mathbf{k}}^{(1)} \\ \Phi_{c\mathbf{k}}^{(2)} \end{pmatrix} = \frac{e^{i\theta_{c\mathbf{k}}}}{\sqrt{2}} \begin{pmatrix} \alpha_{\mathbf{k}} e^{-i\phi_{\mathbf{k}}/2} \\ \beta_{\mathbf{k}} e^{i\phi_{\mathbf{k}}/2} \end{pmatrix}, \tag{7}$$

$$\Phi_{v\mathbf{k}} = \begin{pmatrix} \Phi_{v\mathbf{k}}^{(1)} \\ \Phi_{v\mathbf{k}}^{(2)} \end{pmatrix} = \frac{e^{i\theta_{v\mathbf{k}}}}{\sqrt{2}} \begin{pmatrix} \beta_{\mathbf{k}} e^{-i\phi_{\mathbf{k}}/2} \\ -\alpha_{\mathbf{k}} e^{i\phi_{\mathbf{k}}/2} \end{pmatrix}, \tag{8}$$

where

$$\alpha_{\mathbf{k}} = \sqrt{\frac{\varepsilon_{c\mathbf{k}} + \Delta}{\varepsilon_{c\mathbf{k}}}}, \quad \beta_{\mathbf{k}} = \sqrt{\frac{\varepsilon_{c\mathbf{k}} - \Delta}{\varepsilon_{c\mathbf{k}}}}, \tag{9}$$

$$\phi_{\mathbf{k}} = \tan^{-1}\left(\frac{k}{\kappa_{\nu m}}\right), \tag{10}$$

and there is also an arbitrary phase factor $\exp(i\theta_{s\mathbf{k}})$ related to gauge invariance.

We now turn to the calculation of the optical properties of the system under consideration. Based on the previous studies,[7,8] one can expect that the optical response of BN-SWNT's to light polarized perpendicular to the nanotube axis is suppressed by a depolarization field, as originally predicted by Ajiki and Ando[23] for single-walled carbon nanotubes (SWCNT's). Therefore, in this paper we focus our attention on parallel polarization, when only the long-axis component $\chi_{yy}^{(1)}$ of the second-rank optical susceptibility tensor $\chi_{ij}^{(1)}$ is needed to describe the linear optical response of BN-SWNT's (further for simplicity we omit the subscripts y). The selection rules for the optical excitations relevant to this polarization follow directly from the conservation law of the quantized angular momentum m, as well as from the fact that the photon momentum is extremely small on the microscopic scale. Based on these simple arguments, one can conclude that in the case of the parallel polarization only the vertical interband transitions, which couple the pairs of the electronic states with the same m, are electrically dipole allowed for each k.

In calculating the susceptibility $\chi^{(1)}(\omega)$ at angular frequency ω, we take as a starting point the Genkin-Mednis dispersion formula for $\chi^{(1)}(\omega)$,[24] obtained by using a general formalism they developed to study the optical response (linear and nonlinear) of a two-band semiconductor system in the dipole approximation. Within the independent nanotube approximation, the expression for $\chi^{(1)}(\omega)$ may be written as

$$\chi^{(1)}(\omega) = -\frac{e^2}{V\hbar} \sum_{\mathbf{k}} \sum_{s} \sum_{s' \neq s} f_0(\varepsilon_{s\mathbf{k}}) \times \left[\frac{X_{ss'}(\mathbf{k}) X_{s's}(\mathbf{k})}{\omega_{s's}(\mathbf{k}) + \omega + i\Gamma} + \frac{X_{ss'}(\mathbf{k}) X_{s's}(\mathbf{k})}{\omega_{s's}(\mathbf{k}) - \omega - i\Gamma} \right]. \tag{11}$$

In this equation, V is the normalized volume of the system, $-e$ is the electron charge, $\hbar\omega_{s's}(\mathbf{k}) = \varepsilon_{s'\mathbf{k}} - \varepsilon_{s\mathbf{k}}$ is the energy distance between the bands s and s' at fixed value of $\mathbf{k}$, Γ is a phenomenological broadening factor regularizing the resonant divergencies, which is assumed to be independent of $\mathbf{k}$, $f_0(\varepsilon_{s\mathbf{k}})$ is the Fermi-Dirac distribution function, and X denotes the part of the electron coordinate operator in the crystal momentum representation, which is diagonal only in $\mathbf{k}$. Therefore, the matrix element of the dipole transition between the s and s' bands is

$$X_{ss'}(\mathbf{k}) = \int u_{s\mathbf{k}}^{*}(\mathbf{r}) \partial_{\mathbf{k}} u_{s'\mathbf{k}}(\mathbf{r}) d^3r, \tag{12}$$

where $u_{s\mathbf{k}}(\mathbf{r})$ is the periodic part of the Bloch eigenfunction.

Following the approach developed by Král *et al.*,[11] we can approximately express the Bloch amplitude $u_{s\mathbf{k}}^{(K)}(\mathbf{r})$ around the K point in terms of the periodic parts $u_{\mathbf{K}}^{(1)}(\mathbf{r})$ and $u_{\mathbf{K}}^{(2)}(\mathbf{r})$ of the band-edge Bloch functions as follows:

$$u_{s\mathbf{k}}^{(K)}(\mathbf{r}) = \sum_{j=1,2} \Phi_{s\mathbf{k}}^{(j)} u_{\mathbf{K}}^{(j)}(\mathbf{r}), \tag{13}$$

where the expression for $u_{\mathbf{K}}^{(j)}(\mathbf{r})$ can be established on the basis of the tight-binding approximation as

$$u_{\mathbf{K}}^{(j)}(\mathbf{r}) = \frac{1}{\sqrt{N}} \sum_{n} e^{-i\mathbf{K}\cdot(\mathbf{r}-\mathbf{R}_n-\mathbf{d}_j)} \varphi(\mathbf{r} - \mathbf{R}_n - \mathbf{d}_j). \tag{14}$$

Here N is the total number of the sites occupied by B and N atoms, which is given by

$$N = 2AL \Big/ \left(\frac{\sqrt{3}}{2} a_0^2\right) = \frac{4AL}{\sqrt{3}a_0^2}, \tag{15}$$

where A is the length of the nanotube, L its circumference length, $(\sqrt{3}/2)a_0^2$ is the area of the BN sheet unit cell, and the factor of 2 takes into account that there are two atoms in the unit cell. The function $\varphi(\mathbf{r}-\mathbf{R}_n-\mathbf{d}_j)$ in Eq. (14) is the wave function of a normalized π orbital for an atom located at $\mathbf{R}_n+\mathbf{d}_j$, $\mathbf{R}_n$ and $\mathbf{d}_j$ being the position vectors of the nth unit cell and the jth site in it, respectively.

In our work we are concerned with the situation in which thermal effects are not important, so we can take $f_0(\varepsilon_{s\mathbf{k}})$ in Eq. (11) to be equal to 1 for the occupied electronic states of the v band and 0 for the unoccupied states of the c band. In this case, we then have

$$\chi^{(1)}(\omega) = \frac{e^2}{V\hbar} \sum_{m=-(l-1)}^{l-1} \sum_{k} |X_{cv}(\mathbf{k})|^2 \left[\frac{1}{\omega_{cv}(\mathbf{k}) - \omega - i\Gamma} + \frac{1}{\omega_{cv}(\mathbf{k}) + \omega + i\Gamma} \right]. \tag{16}$$

Using Eqs. (7)–(10) and (12)–(14), one obtains

$$X_{cv}(\mathbf{k}) \equiv X_{cv}(\kappa_{\nu m}, k) = \frac{1}{2} \frac{\gamma^2}{\varepsilon_{c\mathbf{k}} \sqrt{\varepsilon_{c\mathbf{k}}^2 - \Delta^2}} \left(\frac{\Delta}{\varepsilon_{c\mathbf{k}}} k - i\kappa_{\nu m} \right) e^{-i(\theta_{c\mathbf{k}} - \theta_{v\mathbf{k}})} \tag{17}$$

and, hence,

$$|X_{cv}(\mathbf{k})|^2 = \frac{\gamma^2 \Delta_{\nu m}^2}{4\varepsilon_{c\mathbf{k}}^4}. \tag{18}$$

In the limit when the length of the nanotubes goes to infinity, with $\sigma = A/V$ held constant, we can replace the summation over k in Eq. (16) by integration over the same variable. The above-mentioned equation can be separated into real and imaginary parts, and using Eqs. (4), (5), and (17), after some algebraic manipulations we obtain a lengthy but tractable result:

$$\mathrm{Re}\,\chi^{(1)}(\omega) = \frac{e^2 \gamma \sigma}{\pi \Delta^2} \sum_{m=-(l-1)}^{l-1} \frac{1}{a_{\nu m}} \int_0^{c_{\nu m}} (1+t^2)^{-3} (1-t^2)^3 \times [Q_{1\nu m}(z,t) Q_{2\nu m}(\delta, z, t) + Q_{1\nu m}(-z,t) Q_{2\nu m}(\delta, -z, t)] dt, \tag{19}$$

$$\mathrm{Im}\,\chi^{(1)}(\omega) = \delta \frac{e^2 \gamma \sigma}{\pi \Delta^2} \sum_{m=-(l-1)}^{l-1} \frac{1}{a_{\nu m}} \int_0^{c_{\nu m}} (1+t^2)^{-3} (1-t^2)^4 \times [Q_{2\nu m}(\delta, z, t) - Q_{2\nu m}(\delta, -z, t)] dt, \tag{20}$$

where $z = \hbar\omega/2\Delta$ and $\delta = \hbar\Gamma/2\Delta$ are the dimensionless photon energy and the dimensionless broadening constant, respectively. In addition, the following notations are used:

$$Q_{1\nu m}(z,t) = a_{\nu m}(1+t^2) - z(1-t^2), \tag{21}$$

$$Q_{2\nu m}(\delta, z, t) = [Q_{1\nu m}^2(z,t) + \delta^2 (1-t^2)^2]^{-1}, \tag{22}$$

$$a_{\nu m} = \frac{\Delta_{\nu m}}{\Delta} = \sqrt{1 + \frac{\gamma^2 \kappa_{\nu m}^2}{\Delta^2}}, \tag{23}$$

$$b_{\nu m} = \sqrt{a_{\nu m}^2 + \frac{\gamma^2 k_{\mathrm{BZ}}^2}{\Delta^2}}, \tag{24}$$

$$c_{\nu m} = \sqrt{\frac{b_{\nu m} - a_{\nu m}}{b_{\nu m} + a_{\nu m}}}. \tag{25}$$

Although Eqs. (19) and (20) involve only elementary functions, it does not seem possible to calculate $\chi^{(1)}(\omega)$ analytically for any ω values, except the limiting case $\omega \to 0$, which is considered below. However, these equations enable numerical results for $\chi^{(1)}(\omega)$ at an arbitrary ω value to be readily obtained and those are shown in Sec. III.

In the long-wavelength limit ($\omega \to 0$), where $\mathrm{Im}\,\chi^{(1)} = 0$, the integration with respect to t, involved in Eq. (19), can easily be carried out analytically to yield the following simple formula for the important quantity $\chi^{(1)}(0)$, which appears when evaluating the index of refraction $n_0 \equiv n(\omega = 0) = \sqrt{1 + 4\pi\chi^{(1)}(0)}$ in the transparency region:

$$\chi^{(1)}(0) = \frac{2e^2 \gamma \sigma}{3\pi\Delta^2} f_l^{(\nu)}\left(\frac{\Delta}{\gamma k_{\mathrm{BZ}}} \right), \tag{26}$$

with

$$f_l^{(\nu)}\left(\frac{\Delta}{\gamma k_{\mathrm{BZ}}} \right) = \sum_{m=-(l-1)}^{l-1} F\left(\frac{\Delta}{\gamma k_{\mathrm{BZ}}}, \frac{\kappa_{\nu m}}{k_{\mathrm{BZ}}} \right), \tag{27}$$

where the function $F(x,y)$ is defined as

$$F(x,y) = \frac{1 + (3x^2/2) + (3y^2/2)}{(1 + y^2/x^2)(1 + x^2 + y^2)^{3/2}}. \tag{28}$$

Note that in the case when only interband transitions between the two azimuthal subbands with $m = 0$ are taken into account, Eq. (26) can be reduced to the formula obtained for the zero-frequency susceptibility $\chi^{(1)}(0)$ in Ref. 13.

To determine the observed optical properties of BN-SWNT's we need to know the complex optical dielectric function $\varepsilon(\omega) = \varepsilon_1(\omega) + i\varepsilon_2(\omega)$, where the real $\varepsilon_1(\omega)$ and imaginary $\varepsilon_2(\omega)$ parts of $\varepsilon(\omega)$, connected with each other by the Kramers-Kronig relation, are defined as

$$\varepsilon_1(\omega) = 1 + 4\pi\,\mathrm{Re}\,\chi^{(1)}(\omega), \tag{29}$$

$$\varepsilon_2(\omega) = 4\pi\,\mathrm{Im}\,\chi^{(1)}(\omega). \tag{30}$$

It is also convenient to express $\varepsilon(\omega)$ in terms of the complex refractive index $N(\omega) = n(\omega) + i\kappa(\omega)$:

$$\varepsilon(\omega) = [N(\omega)]^2 = [n(\omega) + i\kappa(\omega)]^2, \tag{31}$$

where $n(\omega)$ is the linear real refractive index defined by

$$n(\omega) = \frac{1}{\sqrt{2}} [\varepsilon_1(\omega) + \sqrt{\varepsilon_1^2(\omega) + \varepsilon_2^2(\omega)}]^{1/2} \tag{32}$$

and $\kappa(\omega)$ is the extinction coefficient,

$$\kappa(\omega) = \frac{1}{\sqrt{2}} [-\varepsilon_1(\omega) + \sqrt{\varepsilon_1^2(\omega) + \varepsilon_2^2(\omega)}]^{1/2}. \tag{33}$$

The normal incidence reflectance $\mathcal{R}(\omega)$ may then be calculated using the equation

$$\mathcal{R}(\omega) = \frac{[n(\omega) - 1]^2 + \kappa^2(\omega)}{[n(\omega) + 1]^2 + \kappa^2(\omega)}, \tag{34}$$

while the optical absorption coefficient $\mathcal{K}(\omega)$ is given in terms of the above quantities by

$$\mathcal{K}(\omega) = \frac{\omega}{c} \frac{\varepsilon_2(\omega)}{n(\omega)}, \tag{35}$$

where c is the speed of light in free space.

III. THE CALCULATED OPTICAL SPECTRA

To numerically calculate the optical functions defined by Eqs. (29)–(35), it is first of all needed to choose the appropriate values of the two parameters involved in the KMT model: namely, γ and Δ. In this paper, we adopt the values of $\gamma=5.9$ eV Å and $\Delta=2.2$ eV, which are similar to those used in Ref. 12. Note that the value of $2\Delta=4.4$ eV exactly corresponds to the energy position of the first substructure of the lowest absorption band observed in the experiment.[5] The above value is very close to that predicted by the density-functional-theory calculations for the band gap of zigzag BN-SWNT's[25–27] and is in the range of the experimental energy-band-gap values reported in the literature.[28–30]

There is one more parameter entering the above formulas—namely, $\hbar\Gamma$—which describes the broadening of the spectral resonances due to the finite lifetime of the excited electronic states. Its precise assessment would require more experimental information on the energy relaxation rate in BN-SWNT's than it is available at present. Therefore, in the numerical calculations below, we adopt the value $\hbar\Gamma=44$ meV, which, though reasonable, is rather arbitrary. We have verified that, on varying $\hbar\Gamma$ around the above value, only the width and the height of the peaks in the optical spectra are changed, as should be expected. In this connection, we would like to stress that it is not our objective at this stage to strive towards an agreement with the experiment[5] with respect to the profile of the absorption lines. The point is that the experimental lines seem to be inhomogeneously broadened because of the presence of tubes with various diameters and chiralities in the BNNT sample used in the experiment. However, the real distribution of the nanotube geometry parameters in the sample is unknown, so that at present it does not seem possible to carry out meaningful calculations of the ensemble average of the optical functions. Besides this, although the details of the structure of the sample were not reported in Ref. 5, the authors of that paper mentioned that it contained a small fraction of the material in the form of different kind of nanoparticles, in particular hexagonal boron nitride ($h-$BN) particles. Meanwhile, one of the ultimate goals of modern BNNT production technologies is the fabrication of highly ordered arrays of identical BNNT's. Although at present this goal is still beyond our reach, a first step in this direction has already been made (see, e.g., Ref. 30), and one can hope that, with the improvement of experimental conditions and techniques, such arrays of BN-SWNT's with a uniform diameter and a uniform helical angle will be available. Our analytical results presented above are, strictly speaking, valid for just such ensembles of BN-SWNT's with the zigzag structure of 0° helicity. Actual numerical calculations of the optical functions have been performed for five representative ensembles of this type, consisting, respectively, of BN-SWNT's with indices (15,0), (17,0), (18,0), (19,0), and (21,0). The diameters of these tubes are 1.20, 1.35, 1.43, 1.52, and 1.67 nm, respectively. Hence, it is a (18,0) tube that has a diameter very close to the average diameter of the tubes used in the experiment.[5] Our calculated optical spectra are shown in Figs. 3–5, which we discuss further below.

However, we first consider the easiest functions to understand: namely, the static dielectric constant $\varepsilon_0=1+4\pi\chi^{(1)}\times(0)$ and the index of refraction $n_0=\sqrt{\varepsilon_0}$ at zero frequency—i.e., in the transparency region. Based upon Eq. (26), we have calculated ε_0 and n_0 for ensembles of identical BN-SWNT's with indices from (7,0) to (25,0). The results are presented in Fig. 2. The values of ε_0 and n_0 are plotted for three types of ensembles differing from one another by the way the tubes are arranged. The first type corresponds to densely packed tubes without gaps between them. In this case the surface concentration σ of aligned BN-SWNT's in the plane perpendicular to the longitudinal axis of the nanotubes is given by

$$\sigma = 1/\pi R^2. \tag{36}$$

The two remaining types of ensembles correspond to arrays of the same nanotubes arranged in two-dimensional quadratic and triangular lattices, respectively, with the lattice constant d approximately equal to the interlayer distance of 3.34 Å in h-BN. For a BN-SWNT array with a square-lattice structure, the σ is given by

$$\sigma = 1/(2R+d)^2, \tag{37}$$

whereas in the case of a triangular-lattice structure,

$$\sigma = 2/\sqrt{3}(2R+d)^2. \tag{38}$$

Note that the possibility of the formation of crystalline bundles of BNNT's with a squarelike structure has recently been confirmed experimentally,[30] while a triangular-lattice structure for such bundles is hypothetical (cf. the inverse situation for carbon nanotube bundles[31]) and is considered

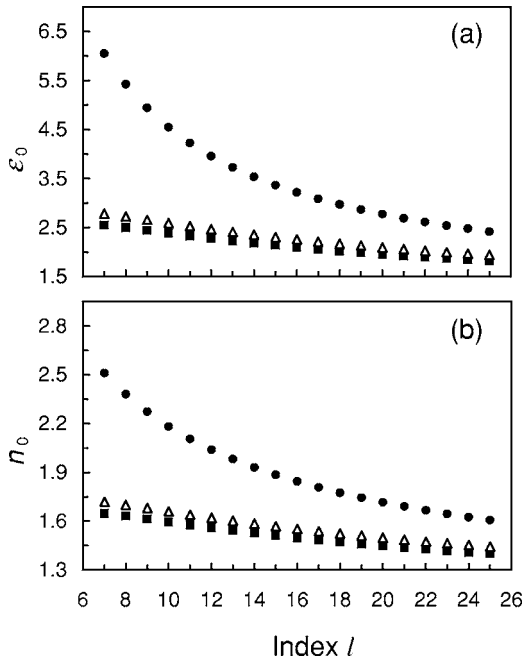

FIG. 2. (a) Static dielectric constant ε_0 calculated for uniform ensembles of BN-SWNT's $(l,0)$ with l ranging from 7 to 25 and (b) refractive index n_0 at zero frequency for the same ensembles. Solid dots, square, and open triangles show the results obtained for the three types of BN-SWNT ensembles specified by Eqs. (36)–(38), respectively.

here for illustrative purposes. It should also be noted that, within the independent nanotube approximation we have used, only the density of nanotubes per unit cross area, defined by the above equations, is relevant here, affecting the magnitude of the zero-frequency linear susceptibility $\chi^{(1)}(0)$ in accordance with Eq. (26).

Our theoretical data in Fig. 2 clearly indicate the tendency of both ε_0 and n_0 to decrease with increasing the nanotube radius R (or with increasing l) for all the three types of ensembles considered, the ε_0 values, as well the n_0 ones, being almost identical for the quadratic- and triangular-lattice structures. Compared to the last ones, the closely packed structure of BN-SWNT's exhibits a considerable enhancement of ε_0 and n_0 for small-diameter tubes. This results from the combination of Eqs. (26) and (36). The function $f_l^{(\nu)}(\Delta/\gamma k_{\mathrm{BZ}})$ in Eq. (26) for the zero-frequency susceptibility $\chi^{(1)}(0)$ depends on R via the parameter $\kappa_{\nu m}$ [see Eq. (6)], but only weakly because of the specific form of the function $F(x,y)$ in Eq. (28). Therefore, the susceptibility $\chi^{(1)}(0)$ of the ensemble of the closely packed BN-SWNT's turns out to be actually inversely proportional to the square of the nanotube radius and, consequently, significantly increases with decreasing R. However, in this connection, a word of caution is in order. The results of our calculation are, in general, less reliable for the smallest BN-SWNT's, since the effects caused by the finite tube curvature (such as $\sigma-\pi$ hybridization and the misalignment of the π orbitals at nearest-neighbor atoms) are left out of account in the KMT model used above. These effects are negligibly small for BN-SWNT's of somewhat large diameters (more than, say, 1 nm), but they, certainly, may turn out to be important for extra-small-diameter tubes, which we are not considering here.

It is noteworthy that the behavior of ε_0 and n_0 for an ensemble of closely packed BN-SWNT's is quite different from that predicted for SWCNT bundles of similar structure, where ε_0 and n_0 are shown to be independent of R.[14,15] This directly reflects the difference between the electronic structures of these two types of nanotubes: conrary to the BN-SWNT's, which are wide-gap semiconductors with an almost constant band gap independent of their diameters, the semiconducting SWCNT's have a band gap which is approximately inversely proportional to the nanotube diameter.

Looking back at Fig. 2, it is also worthwhile to note that the difference in the behavior of ε_0 and n_0 for the three above-mentioned BN-SWNT structures indicates a possible way to discriminate between the closely packed structure of the tubes and the quadratic (or triangular) one by measuring the refractive index of the BN-SWNT sample in the transparency region. A similar possibility for SWCNT samples fabricated in the form of thin films has recently been realized in an experiment by Tatsuura *et al.*[32]

Proceeding to the optical spectra presented in Figs. 3–6, it should be noted that they have been calculated by combining Eq. (36) with Eqs. (19) and (20) and, thus, are formally relevant to ensembles of the closely packed BN-SWNT's. However, the basic qualitative features of the spectra are insensitive to how the tubes are packed in the ensembles, because the density σ enters Eqs. (19) and (20) only as a proportionality factor. Therefore, the spectra in Figs. 3–6 are representative ones not only for the closely packed nanotube structure, but for the two other above-mentioned structures as well.

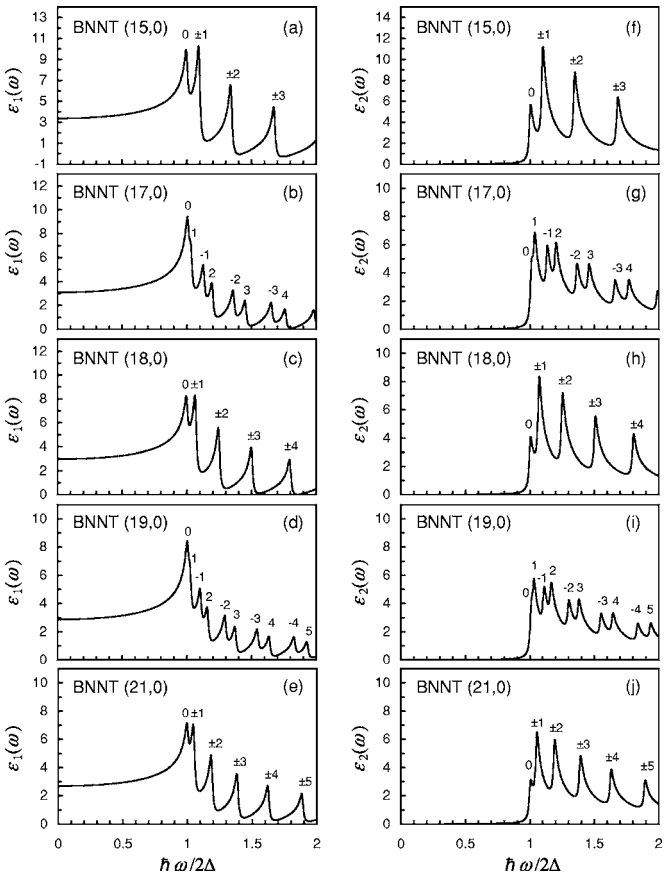

FIG. 3. Theoretical spectra of the real $\varepsilon_1(\omega)$ (left panels) and imaginary $\varepsilon_2(\omega)$ (right panels) parts of the complex dielectric function $\varepsilon(\omega)$ calculated for five uniform BN-SWNT ensembles consisting, respectively, of the tubes with chirality indices (15,0), (17,0), (18,0), (19,0), and (21,0). The latter ones are indicated in the upper part of the panels. The numbers $0,\pm1,\pm2,\ldots$ on the top of the peaks correspond to our labeling convention for the interband electron transitions (for details, see the text).

For the sake of convenience, the optical functions in Figs. 3–6 are plotted versus the dimensionless photon energy $\hbar\omega/2\Delta$. As is clearly seen from these figures, below the threshold value $\hbar\omega/2\Delta=1$ all the spectra are featureless and show a progressive increase of the optical functions as $\hbar\omega/2\Delta$ approaches the threshold. Above it characteristic sharp peaks are observed, which can be attributed to dipole-allowed direct optical transitions between successive pairs of van Hove singularities in the one-dimensional density of states of BN-SWNT's. The mirror pairs of these singularities occur at the edges of the valence and conduction energy subbands with the same azimuthal indices m. The corresponding electron transitions will further be designated by the abbreviation $v_m \rightarrow c_m$, while the corresponding peaks in Figs. 3–6 are labeled simply m $(=0,\pm1,\pm2,\ldots)$. As follows directly from Eqs. (4)–(6), for BN-SWNT's $(l,0)$ with $l=3M$ (further referred to as type-I nanotubes) the energy

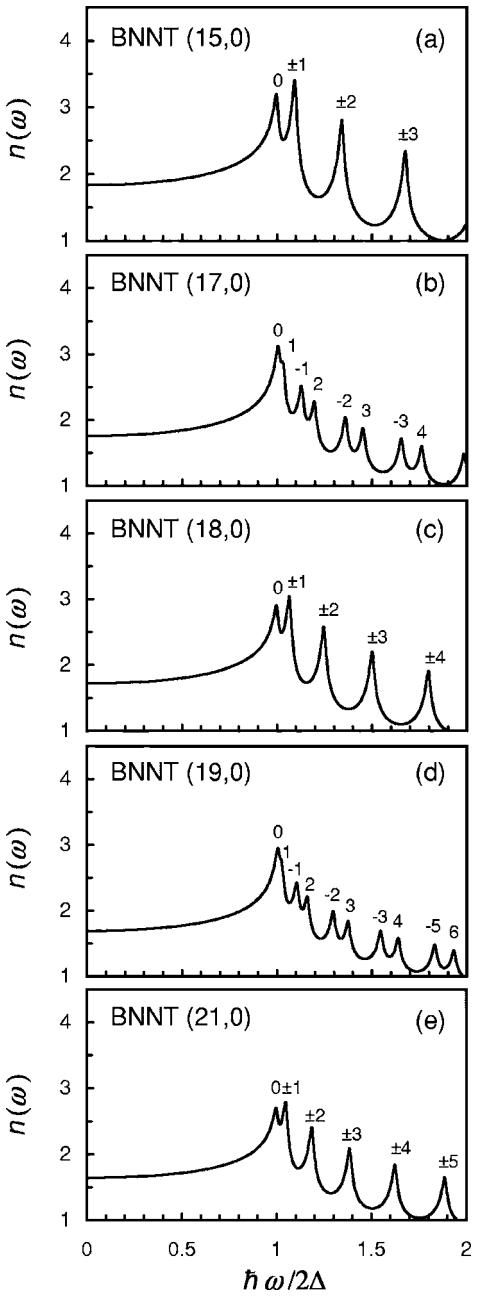

FIG. 4. Calculated spectra of the refractive index $n(\omega)$ for the same BN-SWNT ensembles, as in Fig. 3. Resonant interband electron transitions are indicated by the numbers on the top of the peaks, as in Fig. 3.

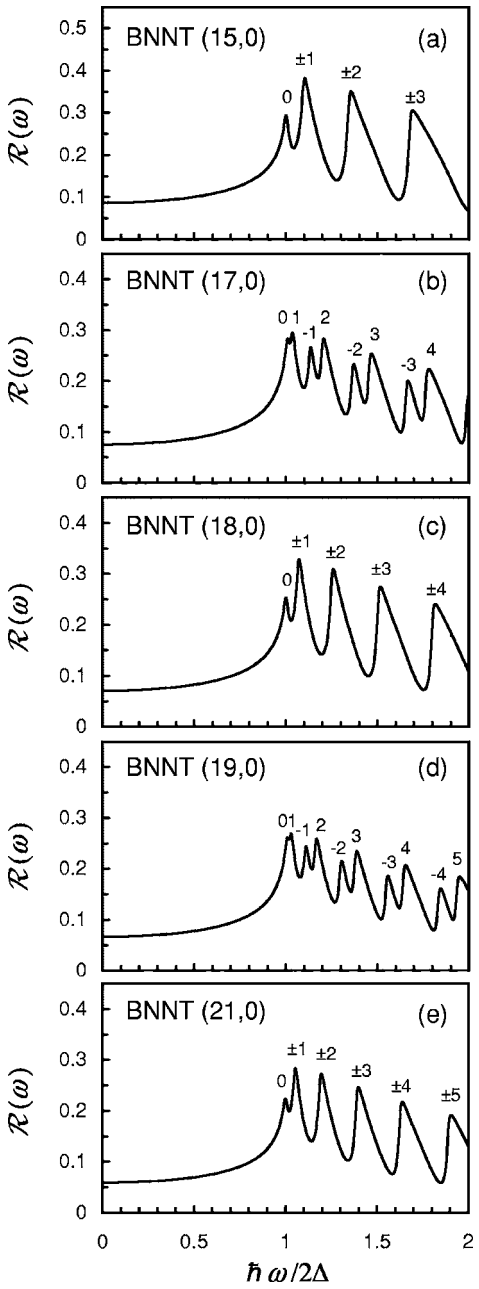

FIG. 5. Calculated spectra of the reflectance $\mathcal{R}(\omega)$ for the same BN-SWNT ensembles, as in Fig. 3. Resonant interband electron transitions are indicated by the numbers on the top of the peaks, as in Fig. 3.

subbands with $m \neq 0$ are doubly degenerate in m for any value of k, but the degeneracy is lifted in the case of BN-SWNT's $(l,0)$ specified by the index $l=3M\pm1$ (further referred to as type-II nanotubes). As a consequence, the number of peaks observed in the optical spectra for the latter type of the nanotubes is larger than that for the former one [cf., for example, Figs. 3(a) and 3(b)]. The overall trend to more peaks, as well as to smaller energy spacing between two neighboring peaks, for thicker tubes belonging to one and the same above-mentioned type of BN-SWNT's is also clearly seen in Figs. 3–6.

Inspection of Fig. 3 shows that there are two important differences in both the $\varepsilon_1(\omega)$ and the $\varepsilon_2(\omega)$ spectra for the type-I and type-II nanotubes. First, as seen from Figs. 3(a), 3(c), and 3(e), the central, most prominent peak in the $\varepsilon_1(\omega)$ spectra of the type-I nanotubes actually consists of two subpeaks of almost equal height, which correspond to $v_0 \rightarrow c_0$ and $v_{\pm1} \rightarrow c_{\pm1}$ transitions, respectively. Contrary to this, the central peak in the $\varepsilon_1(\omega)$ spectra of the type-II nanotubes has no double-peak structure, but it has a narrow shoulder, corresponding to the $v_1 \rightarrow c_1$ transition and situated on the right-hand wing of the peak [see Figs. 3(b) and 3(d)]. Second, the $\varepsilon_1(\omega)$ spectra of the type-I nanotubes exhibit sharply asym-

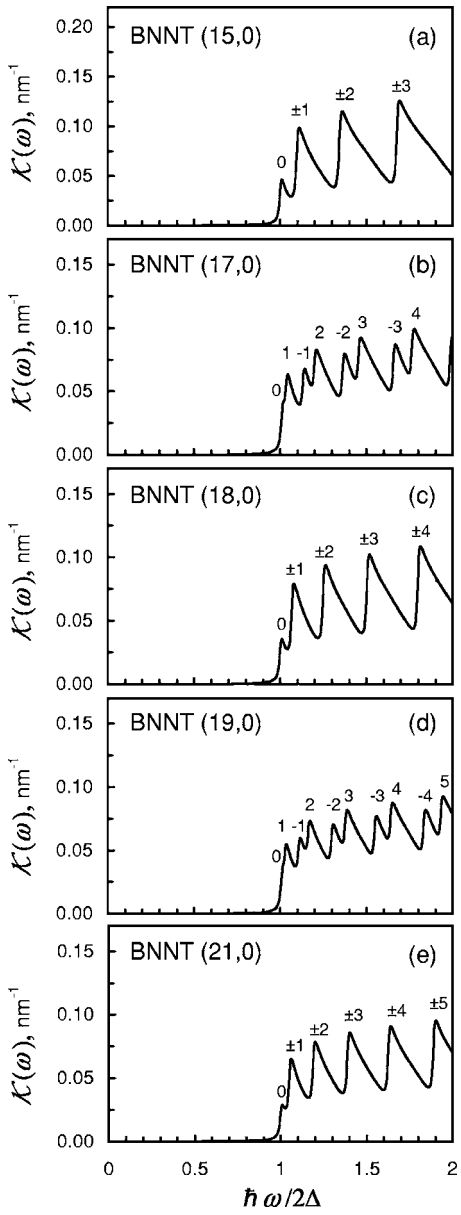

FIG. 6. Calculated optical absorption spectra for the same BN-SWNT ensembles, as in Fig. 3. Resonant interband electron transitions are indicated by the numbers on the top of the peaks, as in Fig. 3.

metrical, deep dip structures situated between all the nearest-neighboring peaks except the first two. In the right-hand neighborhood of the peaks the corresponding $\varepsilon_1(\omega)$ drastically changes from a large positive value to a small positive (or negative) one. Although such dip structures exist in the $\varepsilon_1(\omega)$ spectra of the type-II nanotubes as well, they are shallow rather than deep.

The aforesaid differences in the $\varepsilon_1(\omega)$ spectra of the type-I and type-II nanotubes have their counterparts in the corresponding $\varepsilon_2(\omega)$ spectra. Indeed, as seen from Figs. 3(f)–3(j), the most prominent peak in the $\varepsilon_2(\omega)$ spectra always corresponds to the $v_1 \rightarrow c_1$ transition. However, in the $\varepsilon_2(\omega)$ spectra of the type-I nanotubes there is a nearest-neighboring peak corresponding to the $v_0 \rightarrow c_0$ transition, situated on the left-hand side of the central peak, whereas for the type-II nanotubes a narrow shoulder is observed instead of the former peak. Besides this, we again observe deep dip structures in the $\varepsilon_2(\omega)$ spectra of the type-I nanotubes and, in contrast, rather shallow ones in the $\varepsilon_2(\omega)$ spectra of the type-II nanotubes.

Finally, there is one more point to be noted regarding the spectra in Fig. 3. The amplitudes of all the peaks in these spectra become smaller as the diameters of the nanotubes become larger. This implies that, if one desires to attain a larger optical response of BN-SWNT ensembles, one should preferably use those fabricated from small-diameter tubes.

The above-mentioned features of the real and the imaginary parts of $\varepsilon(\omega)$ are directly reflected in the $n(\omega)$ and the $\mathcal{R}(\omega)$ spectra, which are shown in Figs. 4 and 5, respectively. In particular, the spectral behavior of $n(\omega)$ is qualitatively the same as for $\varepsilon_1(\omega)$ except for the obvious reduction in the intensity of the dips. Nevertheless, the refractive index $n(\omega)$ of the type-I nanotube ensembles changes rather significantly in the vicinity of the resonances, the number of which, in its turn, depends on the diameter of the nanotube. This means that the $n(\omega)$ spectra could be used in experiment to identify the preferred nanotube geometry in a BN-SWNT ensemble. It is also interesting to note the just above the threshold $\hbar\omega/2\Delta=1$ the peak values of $n(\omega)$ are rather large ($n_{\max} \approx 3$) for the smallest nanotubes considered. It is well known (see, e.g., Ref. 33) that the linear refractive index $n(\omega)$ enters the figure of merit of electro-optical materials. The above-mentioned relatively large peak values of $n(\omega)$, as well as a relatively large refractive-index change in the vicinity of the resonances, indicate that BN-SWNT's are possibly a suitable material to be used in the design of nanoscale optoelectronic devices, such as, for example, electro-optical modulators in the ultraviolet region.

Turning next to Fig. 5, we find the characteristic peak and dip structures, the spectral position of the former being related to the energetic separation between pairs of van Hove singularities in the electronic density of states of both the types of BN-SWNT's. Again we observe that the details of the behavior of $\mathcal{R}(\omega)$ are sensitive to the types of the nanotubes, but the overall trend is that the reflectance $\mathcal{R}(\omega)$ decreases with increasing the nanotube diameter. Comparing Figs. 5 and 6, it is also worth noting that experimental measurements of the reflectance spectra, which directly display the sharp characteristic features corresponding to the interband transitions above the threshold $\hbar\omega/2\Delta=1$, might also be useful to investigate an opaque BN-SWNT sample in the ultraviolet region below the threshold, which is inaccessible to the optical absorption spectroscopy.

We finally turn to a discussion of the calculated optical absorption spectra displayed in Fig. 6, which show the characteristic resonances associated with the electron transitions between the occupied valence-band states and the unoccupied conduction-band ones. It is interesting to note that the spectral profiles of the resonances in this figure, as well as their relative strength, are markedly different from those in the $\varepsilon_2(\omega)$ spectra, reflecting the effect of the refractive-index dispersion on the absolute strength and the shape of the optical resonances. In particular, the resonances observed in

Fig. 6 are apparently more broadened and asymmetrical than those in Figs. 3(f)–3(j), exhibiting a sawtoothlike behavior. This is a direct consequence of rather broad dip structures in the $n(\omega)$ spectra (see Fig. 4). Furthermore, the presence of $n(\omega)$ in the denominator of Eq. (35) for the absorption coefficient $\mathcal{K}(\omega)$ reverses the relative intensity of the second and the subsequent peaks in the $\mathcal{K}(\omega)$ spectra as compared to their relative intensity in the $\varepsilon_2(\omega)$ spectra [cf. Figs. 6 and 3(f)–3(j)]. Thus, our calculations reproduce the finding of Lauret *et al.*[5] that the second and third absorption bands in the observed optical spectrum have larger peak intensities than both the substructures of the first band.

As has already been mentioned, a BN-SWNT (18,0) has a diameter which is very close to the average diameter of the tubes used in the experiment by Lauret *et al.*[5] For an ensemble of such tubes, it follows from Fig. 6(c) that the first four absorption peaks occur at 4.4, 4.7, 5.6, and 6.7 eV, respectively. These values are in reasonable agreement with the experimental peak energy values of 4.4, 4.5, 5.5, and 6.15 eV.[5] The calculated spectrum in Fig. 6(c) also correctly reproduces the experimental observation by Lauret *et al.*[5] that the absorption substructure at 4.4 eV possesses a smaller strength than that at 4.5 eV. In this regard our calculations agree with the experimental data better than any others published to date and place theory and experiment in good qualitative agreement. However, there are some discrepancies between the theoretical results and the experimental ones with respect to the peak energy positions as well as to the shape of the peaks in the spectrum. Some differences may come from the simplifications involved in the theory as well as from uncertainties in the values of the two relevant parameters γ and Δ entering the KMT model we used. Indeed, the above chosen values of these parameters, although reasonable, are not known exactly. As to the simplifications used in the theory, it should be noted that the calculations going beyond the independent-particle approximations and including electron-electron repulsion and electron-hole attraction may have only a relatively small net effect on the peak energy positions,[9,10] which can be taken into account by phenomenologically adjusting the parameter Δ. In addition, some discrepancies between theory and experiment can be attributed to experimental uncertainties in the measured peak energy positions as well to the fact that the experimental sample contained BN-SWNT's of different diameters. In the context of the above discussion, we would like to remind the reader that our primary intention in this paper is not to explain completely the absorption spectrum observed experimentally, but rather to investigate to what extent a simple one-electron-theory approach, disregarding exchange-correlation effects, is able to provide a qualitative understanding of the optical properties of BN-SWNT's. Our calculations presented above clearly demonstrate that the KMT model of the electronic structure of BN-SWNT's, based on a single-particle approximation, offers a convenient, physically motivated scheme for studying such properties and the results thereof can form a reasonable background for future theoretical studies. We believe that these along with even more controlled experimental optical-absorption studies, carried out on BN-SWNT samples containing monosized and well-aligned nanotubes, may yield a somewhat better agreement between theory and experiment than has been achieved in this paper.

IV. SUMMARY

In this work, we have investigated theoretically the linear optical properties of zigzag BN-SWNT's of different diameters. We have considered a number of uniform ensembles of such tubes and developed an approach that allows one to treat their optical response more or less analytically. The Král-Mele-Tománek effective Hamiltonian[11] has been used to model the electron energy dispersion and the single-electron eigenstates of the system. Within this model, explicit analytical formulas [Eqs. (19) and (20)] have been obtained for the real and imaginary parts of the linear optical susceptibility $\chi^{(1)}(\omega)$, which have been used to calculate numerically the spectra of the dielectric function $\varepsilon(\omega)$, the refractive index $n(\omega)$, the reflectance $\mathcal{R}(\omega)$, and the optical absorption coefficient $\mathcal{K}(\omega)$ of BN-SWNT ensembles containing tubes of somewhat large diameters ($\geqslant$1.2 nm). All these spectra have been shown to exhibit prominent characteristic peaks associated with interband electron transitions between pairs of van Hove singularities in the electronic density of states of the tubes. The calculated optical absorption spectra have been compared with the experimental spectrum measured by Lauret *et al.*[5] for an assembly of BN-SWNT's with an average diameter of about 1.4 nm. It has been found that our theoretical spectrum for an ensemble of BN-SWNT's (18,0) with a diameter of 1.43 nm qualitatively reproduces the characteristic features observed experimentally in Ref. 5. However, some discrepancies between theory and experiment still exist, and further experimental and theoretical developments are needed to achieve a complete understanding of the optical properties of BN-SWNT's. In particular, the importance of excitonic effects in BN-SWNT's is still an open question, and only the experiments have to decide the controversy regarding the nature of the optical transitions in these novel materials.

To conclude, we should stress we are not claiming that a one-electron-theory approach, which we have relied on in this paper, suffices to describe all the details of the optical response of BN-SWNT's. However, it is striking to realize the very good first-order description that such a theory is able to provide for the experimental data. This feature should be borne in mind when the results of more refined calculations are discussed.

ACKNOWLEDGMENTS

The research by Vl.A.M. and E.A.G. was supported by the RFBR. In addition, one of the authors (O.V.B.) acknowledges support from the Grant Counsel of the President of the Russian Federation for Young Scientists.

*Corresponding author. Present address: Sovetskaya 31, kv.32, Saransk 430000, Russia. Electronic address: 612033@inbox.ru

[1] A. Rubio, J. L. Corkill, and M. L. Cohen, Phys. Rev. B **49**, 5081 (1994).
[2] X. Blase, A. Rubio, S. G. Louie, and M. L. Cohen, Europhys. Lett. **5**, 335 (1994).
[3] N. G. Chopra, R. J. Luyken, V. H. Crespi, M. L. Cohen, S. G. Louie, and A. Zettl, Science **269**, 966 (1995).
[4] L. Boulanger, B. Andriot, M. Cauchetier, and F. Willaime, Chem. Phys. Lett. **234**, 227 (1995).
[5] J. S. Lauret, R. Arenal, F. Ducastelle, A. Loiseau, M. Cau, B. Attal-Tretout, and E. Rosencher, Phys. Rev. Lett. **94**, 037405 (2005).
[6] M.-F. Ng and R. Q. Zhang, Phys. Rev. B **69**, 115417 (2004).
[7] A. G. Marinopoulos, L. Wirtz, A. Marini, V. Olevano, A. Rubio, and L. Reining, Appl. Phys. A: Mater. Sci. Process. **78**, 1157 (2004).
[8] G. Y. Guo and J. C. Lin, Phys. Rev. B **71**, 165402 (2005).
[9] C.-H. Park, C. D. Spataru, and S. G. Louie, Phys. Rev. Lett. **96**, 126105 (2006).
[10] L. Wirtz, A. Marini, and A. Rubio, Phys. Rev. Lett. **96**, 126104 (2006).
[11] P. Král, E. J. Mele, and D. Tománek, Phys. Rev. Lett. **85**, 1512 (2000).
[12] E. J. Mele and P. Král, Phys. Rev. Lett. **88**, 056803 (2002).
[13] A study on this subject with preliminary results for a representative BNNT was presented by the authors as a conference proceedings in Vl. A. Margulis, O. V. Boyarkina, L. V. Fomina, E. A. Gaiduk, and E. E. Muryumin, Fullerenes, Nanotubes, Carbon Nanostruct. **14**, 239 (2006).
[14] Vl. A. Margulis and E. A. Gaiduk, Phys. Lett. A **281**, 52 (2001).
[15] Vl. A. Margulis and E. A. Gaiduk, Chem. Phys. Lett. **341**, 16 (2001).
[16] A. Fujiwara, Y. Matsuoka, H. Suematsu, N. Ogawa, K. Miyano, H. Kataura, Y. Maniwa, S. Suzuki, and Y. Achiba, Jpn. J. Appl. Phys., Part 2 **40**, L1229 (2001).
[17] M. F. Islam, D. E. Milkie, C. L. Kane, A. G. Yodh, and J. M. Kikkawa, Phys. Rev. Lett. **93**, 037404 (2004).
[18] C. L. Kane and E. J. Mele, Phys. Rev. Lett. **93**, 197402 (2004).
[19] E. B. Barros, R. B. Capaz, A. Jorio, G. G. Samsonidze, A. G. Souza Filho, S. Ismail-Beigi, C. D. Spataru, S. G. Louie, G. Dresselhaus, and M. S. Dresselhaus, Phys. Rev. B **73**, 241406(R) (2006).
[20] F. Wong, G. Dukovic, L. E. Brus, and T. F. Heinz, Science **308**, 838 (2005).
[21] M. Terauchi, M. Tanaka, K. Suzuki, A. Ogino, and K. Kimura, Chem. Phys. Lett. **324**, 359 (2000).
[22] R. S. Lee, J. Gavillet, M. Lamy de la Chapelle, A. Loiseau, J.-L. Cochon, D. Pigache, J. Thibault, and F. Willaime, Phys. Rev. B **64**, 121405(R) (2001).
[23] H. Ajiki and T. Ando, Physica B **201**, 349 (1994).
[24] V. M. Genkin and P. M. Mednis, Sov. Phys. JETP **27**, 609 (1968).
[25] T. M. Schmidt, R. J. Baierle, P. Piquini, and A. Fazzio, Phys. Rev. B **67**, 113407 (2003).
[26] H. J. Xiang, J. Yang, J. G. Hou, and Q. Zhu, Phys. Rev. B **68**, 035427 (2003).
[27] S. S. Han, S. H. Lee, J. K. Kang, and H. M. Lee, Phys. Rev. B **72**, 113402 (2005).
[28] R. Czerw, S. Webster, D. L. Carroll, S. M. C. Vieira, P. R. Birkett, C. A. Rego, and S. Roth, Appl. Phys. Lett. **83**, 1617 (2003).
[29] G. G. Fuentes, E. Borowiak-Palen, T. Pichler, X. Liu, A. Graff, G. Behr, R. J. Kalenczuk, M. Knupfer, and J. Fink, Phys. Rev. B **67**, 035429 (2003).
[30] J. Wang, V. K. Kayastha, Y. K. Yap, Z. Fan, J. G. Lu, Z. Pan, I. N. Ivanov, A. A. Puretzky, and D. B. Geohegan, Nano Lett. **5**, 2528 (2005).
[31] R. Saito, G. Dresselhaus, and M. S. Dresselhaus, *Physical Properties of Carbon Nanotubes* (Imperial College Press, London, 1998).
[32] S. Tatsuura, M. Furuki, Y. Sato, I. Iwasa, M. Tian, and H. Mitsu, Adv. Mater. (Weinheim, Ger.) **15**, 534 (2003).
[33] T. S. Moss, G. J. Burrell, and B. Ellis, *Semiconductor Opto-Electronics* (Butterworths, London, 1973).